Smart Structures and Systems, *Vol. 30, No. 5 (2022) 447-462*
https://doi.org/10.12989/sss.2022.30.5.447

Numerical modelling of a shear-thickening fluid damper using optimal transit parameters

Chung-Han Yu [1a], Yohanes K. Surjanto [2b], Pei-Ching Chen*[2], Shen-Kai Peng [1c] and Kuo-Chun Chang [3d]

[1] *National Center for Research on Earthquake Engineering, National Applied Research Laboratories, No. 200, Sec. 3, Xinhai Rd., Da'an Dist., Taipei City 106219, Taiwan*
[2] *Department of Civil and Construction Engineering, National Taiwan University of Science and Technology, No.43, Keelung Rd., Sec.4, Da'an Dist., Taipei City 106335, Taiwan*
[3] *Department of Civil Engineering, National Taiwan University, No. 1, Sec. 4, Roosevelt Rd., Da'an Dist., Taipei City 10617, Taiwan*

(*Received November 9, 2021, Revised July 23, 2022, Accepted August 25, 2022*)

Abstract. The viscosity of a shear-thickening fluid damper (STFD) can increase dramatically when the STFD undergoes high-rate of excitation. Therefore, accurate numerical modelling of the STFD has been considered difficult due to this distinct feature. This study aims to develop a numerical model to accurately simulate the response of the STFD. First, a STFD is designed, fabricated, and installed in the laboratory. Then, performance tests are conducted in which sine waves with nine frequencies at three amplitude levels are adopted as the displacement excitations to the STFD. A novel numerical model which contains two parameter sets of the discrete Bouc-Wen model as well as two parameters for transiting the two parameter sets. Therefore, a total number of eighteen parameters need to be identified in the damper model. The symbiotic organisms search is applied to optimize the parameters. Numerical simulation results demonstrate that the proposed STFD model with transit parameter sets outperforms the conventional discrete Bouc-Wen model. The proposed STFD model can be applied to analyses of structures in which STFDs are installed in the future.

Keywords: numerical modelling; shear-thickening fluid damper; symbiotic organisms search; transit parameters

1. Introduction

Considering the widely applicable fluid-type dampers in seismic engineering field, the efficiency of energy dissipation and vibration mitigation have been verified by a large number of theoretical studies, physical experiments, as well as real seismic responses of buildings, bridges, and other structures. Theoretically, fluid-type dampers feature velocity-dependent force property which directly provides damping to structures without additional stiffness. Therefore, seismic demands in building structures are not affected. Among various fluid-type dampers, viscous dampers (Huang 2018, Lewandowski *et al*. 2017) and oil dampers (Kurino *et al*. 2003) have been commonly applied to real practice as their force-velocity relations can be briefly represented by a well-known equation

$$F = CV^{\alpha} \tag{1}$$

in which F and V refer to the damper force and relative velocity across the damper, respectively; while C and α are the damping coefficient and constant exponent, correspondingly. For seismic engineering applications, viscous dampers with the exponent smaller than one are commonly used since the desired damping force can be reached under small vibration velocity. In other words, damping effect can function when minor earthquake excitation is occurred. For similar application purpose, oil dampers are developed with bilinear force-velocity property, which is similar to that of viscous dampers, by connecting a passive control valve that can be triggered on or off according to the internal liquid pressure.

The damping force of a viscous damper is generated by the liquid pressure difference between two chambers separated by a piston head (Constantinou and Symans 1993). Complex design of piston head with varying cross section of orifices or geometry of tunnels controls the force-velocity property, e.g., the value of exponent α. Alternatively, if a solid piston without any orifices or tunnels inside is adopted, fluid merely passes through the piston from the annular gap between the piston head and cylinder wall. In this case, the filling fluid is an incompressible Newtonian fluid. Theoretically, the exponent value in the force-velocity behaviour is equal to one and the hysteresis loop becomes a perfect ellipse. It is noted that the viscosity of Newtonian fluid is independent of fluid shear rate. However, except for the configuration design of piston head, the filling fluid also controls the property of viscous dampers. The damping force of a damper filled with high-viscosity silicon oil is larger than

*Corresponding author, Associate Professor,
E-mail: peichingchen@mail.ntust.edu.tw
[a] Associate Researcher, E-mail: chyu@narlabs.org.tw
[b] Graduate Student, E-mail: m10805825@mail.ntust.edu.tw
[c] Assistant Researcher, E-mail: skpeng@narlabs.org.tw
[d] Distinguished Professor, E-mail: ciekuo@ntu.edu.tw

ISSN: 1738-1584 (Print), 1738-1991 (Online)

that filled with lower-viscosity silicon oil. It is noteworthy that although silicon oil is a non-Newtonian fluid, it is usually assumed as a Newtonian fluid in design since its viscosity remains in constant under the practical application in earthquake engineering

Nevertheless, in spite of the wide application and appreciated energy dissipation capability of viscous dampers, limitation of single control target occasionally leads to dilemma situations for structural seismic design. For example, viscous dampers are often used in the isolation system to suppress isolation displacement under significant ground motions. If a seismically isolated structure is located at a near-fault area, dampers in the isolation system should be designed with much higher damping coefficient according to the potential large isolation displacement caused by the pulse-like long-period ground motions (Baker 2007). Although this design strategy satisfies safety requirement, such large damping force also suppresses the movement of isolation system under regular or small earthquakes and may greatly reduce the serviceably or even cause unexpected minor structural damages (Providakis 2008). To overcome this dilemma, in recent years, the optimal design strategies of viscous dampers for isolation systems have been widely studied (Guler and Alhan 2019, Bañuelos-García *et al*. 2020). On the other hand, the closed-loop control technology was applied to seismic engineering by using sensing feedback system and controllable energy dissipation devices, such as magneto-rheological (MR) dampers (Zapateiro *et al*. 2010). Its control efficiency could be further enhanced by improving the sensing system to wireless transmission (Linderman and Spencer 2015). Regarding to near-fault earthquakes, the MR dampers controlled by optimal fuzzy rules were verified to reduce structural responses (Ghaffarzadeh 2013). Even for seismically isolated buildings, the semi-active control efficiency was probabilistically discussed (Oncu-Davas and Alhan 2019).

Alternatively, a novel passive control solution to the aforementioned dilemma through material approach has been launched in recent years. From a previous study, it was observed that when suspension fluid was disturbed, tiny particles suspended in the fluid aggregated together, causing a rapid increase to the fluid viscosity (Barne 1989). The aggregation phenomenon was induced by the Van der Waals force between molecules which was verified by Hoffman's experimental and theoretical study (Hoffman 1974). This increase of viscosity was named as shear-thickening behaviour. Actually, the shear-thickening behaviour is a defect that might induce damage to the liquid delivery system in the industrial processing. However, in recent years, researchers aimed to investigate these properties of suspensions and corresponding potential applications by using nanomaterials (Bidgoli *et al*. 2016, Khater 2016). For example, this aforementioned defect can be treated as a material property utilized in the piston system to provide sudden rise of damping force as an additional control mechanism in earthquake engineering studies. In other words, the shear-thickening phenomenon of the non-Newtonian fluid results in damping force with $\alpha > 1$ in low velocity stage.

Recently, several studies were aimed at developing multifunctional passive viscous dampers, which comprised two continuous parts of viscous behaviours with different damping coefficients and exponents (in view of force-velocity property) by using the shear-thickening behaviour of non-Newtonian fluid (Yeh *et al*. 2014, Zhao *et al*. 2018, Wei *et al*. 2019). These studies all adopted non-Newtonian fluids, such as polyethylene glycol (PEG) carrier fluid mixed with nano-scaled fumed silica (SiO_2) particles or polypropylene glycol (PPG) carrier fluid mixed with nano-scaled fumed silica (SiO_2) particles to fill in dampers designed with annular gape around the piston head. According to these studies, by adjusting the types of material and concentration of the suspension fluid, dampers can exhibit various behaviours, such as different damping coefficients and exponents in the force-velocity relationship as well as a critical velocity that divides the exponent into two stages of $\alpha > 1$ and $\alpha < 1$. According to Yeh *et al*.'s theoretical and numerical study, the shear-thickening fluid damper (STFD) possessed an initial behaviour with exponent larger than one ($\alpha > 1$) and continue by a behaviour with exponent smaller than one ($\alpha < 1$). The damping force remains in a small value under small vibration, and rapidly increases during the specific designed velocity threshold. This unique property may be applied in a seismically isolated building to solve the aforementioned dilemma. However, STFDs are still in the developing phase. Damper mechanism and material effects on the damper responses need to be further investigated. In particular, development of an optimal and suitable numerical model of STFDs is critical to realizing the seismic performance of buildings with STFDs. This numerical model should be able to clearly represent the force-displacement behaviour of a STFD from experimental testing, instead of a simple regression of Eq. 1 that was used in the past studies.

In this study, a STFD is designed and fabricated first. Performance tests of the damper are conducted in the laboratory in order to obtain the force-to-displacement responses of the damper. Then, a numerical model based on the discrete-time Bouc-Wen model is proposed and verified to represent the force-to-displacement behaviour of the STFD. Two sets of Bouc-Wen models are optimized together with a transition curve, which is a function of relative velocity at the two ends of the damper, in order to simulate the varying response of the STFD from low velocity to high velocity. A novel metaheuristic optimization method named symbiosis organisms search (SOS) is applied to optimize the parameters of the model with transit parameters (Cheng and Prayogo 2014). As a result, these two sets of parameters are transiting to each other based on the optimal transition curve. Numerical simulation results demonstrate that the proposed numerical model with optimal transit parameters simulate the response of STFD exceptionally. The numerical model can be incorporated into structural analysis of a seismically isolated building for future studies.

(a) AR2000ex rheometer

(b) Loading sample fluid

(c) Conducting rheology test

Fig. 1 Rheology tests of the three samples

2. Design and fabrication of the shear-thickening fluid damper

This section documents the design and fabrication of the STFD used in this study including the rheology tests of shear-thickening fluid with various concentrations, and the design of damper mechanism.

2.1 Shear-thickening fluid

The shear-thickening fluid produced for this study is composed of fumed silica particles (AEROSIL® R972) with 16 nm diameters and 110 ± 20 m^2/g surface area as well as PPG fluid carrier (PPG3000) with molecular weight of 3000 g/mol and density around 1.005 g/ml. The PPG is a Newtonian fluid and an organic compound with the molecular formula of ($H[OCH(CH_3)CH_2]_nOH$), in which the subscript n implies the chain length of the molecular. Longer chain length leads to larger molecular weight and viscosity. As noted by American Agency for Toxic Substances and Disease Registry, the propylene glycol is a "generally recognized as safe" (GRAS) additive for food and medications which rarely causes toxic effects. On the other hand, the fumed silica, which specially refers to the tiny crystal type of silicon dioxide SiO_2 with diameter in the range of 5 nm to 50 nm, is a non-toxic material that is typically used in liquid products to modify the rheology properties, such as paints and white glue. Owing to the facts that both the two materials are stable and durable, as well as the boiling point of PPG is in the range of 230°C to 330°C, the shear-thickening fluid is suitable for the earthquake engineering application.

In order to decide suitable shear-thickening fluid for further performance tests and observe the tendency of rheology properties, three samples with various concentrations were created. The weight percentage of each sample was 4%, 6%, and 8%, respectively. The three shear-thickening fluid samples were named as PPG3000-R972-4%, PPG3000-R972-6%, and PPG3000-R972-8% according to the weight percentage. The three samples were made on a BLDCM BLG-3D digital type blender, which possessed a maximum rotational speed of 750 rpm and provided a maximum of 60 N-cm torque for fluid viscosity smaller than 50 Pa-s by carefully adding a small amount of fumed silica particles into PPG fluid. The AR2000ex

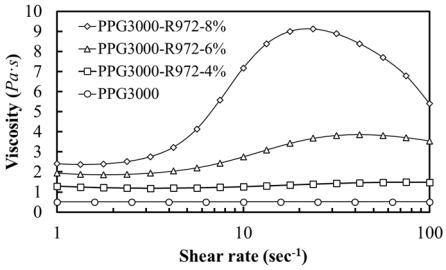

Fig. 2 Rheology properties of shear-thickening fluid samples

rotational type rheometer with cone and plate fixtures produced by TA Instrument, as shown in Fig. 1, was used to carry out the rheology tests. It was necessary to conduct several steady-state tests under various shear rates to obtain an entire rheology curve of one sample which was presented by viscosity and shear rate. Noted that the viscosity and shear rate magnitudes were calculated from the controlled constant rotating speed and measured torque of the upper cone-shaped fixture. Fig. 2 shows the rheology test results which includes the rheology property of pure PPG fluid as the reference of comparison. It can be obviously found that the PPG fluid exhibits Newtonian property. The shear-thickening fluid with low concentration (PPG3000-R972-4%) is similar to Newtonian fluid; however, viscosity is larger than that of the PPG fluid. The concentration increases, the shear-thickening behaviour becomes more significant. Meanwhile, the shear rate magnitude corresponding to the maximum viscosity decreases when the concentration increases. The maximum viscosity and the corresponding shear rate for PPG3000-R972-6% and PPG3000-R972-8% are 3.86 Pa-s and 42.17 sec^{-1}, and 9.12 Pa-s and 12.17 sec^{-1}, respectively. Although the PPG3000-R972-8% fluid possessed more significant shear-thickening phenomenon than the other two, the PPG3000-R972-6% fluid was suitably chosen for the follow-up experimental study considering the range of $\alpha>1$ for the damper performance in the low velocity stage even it might be inconspicuous.

2.2 Shear-thickening fluid damper

A damper with a solid piston head and annular gap was

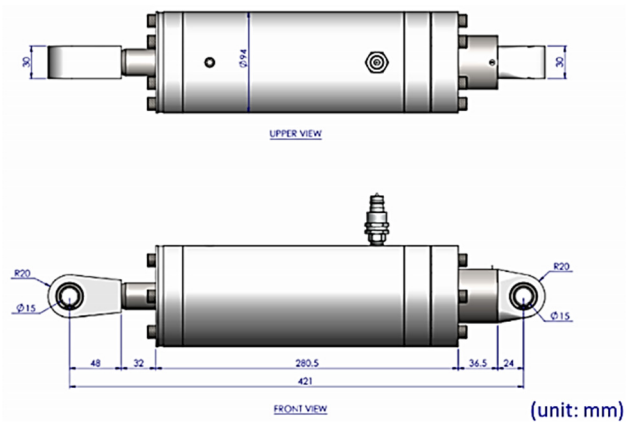

(a) Appearance

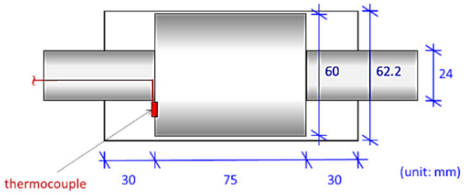

(b) Schematics of inner design

Fig. 3 Configuration design of the shear-thickening fluid damper

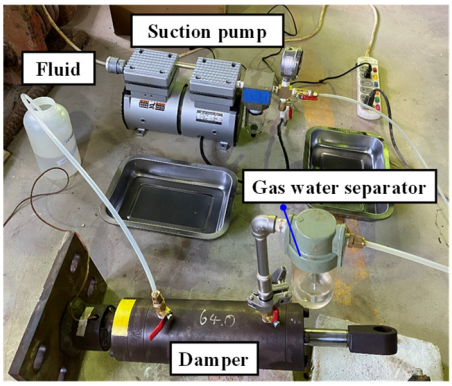

Fig. 4 Vacuum perfusion process of the shear-thickening fluid damper

designed for the performance tests. As illustrated in Fig. 3(a), the damper's total length is 450 mm and the outer diameter of the cylinder is 94 mm. The diameter of the connecting rod, piston head, and inner surface of the cylinder are 24 mm, 60 mm, 62.2 mm, respectively as shown in Fig. 3(b) which indicates that the annular gap is 2.2 mm. On the other hand, the total axial length of the cylinder chamber is 135 mm. The stroke of the damper is ±30 mm which can be calculated by deducting the axial length of piston head. Furthermore, one thermocouple was attached on the end of the piston head to directly monitor the internal temperature in order to reduce the effect of different initial temperatures on the performance test results. Fig. 4 exhibits the perfusion process of the damper with PPG3000-R972-6% fluid. The damper was connected to one container filled with PPG3000-R972-6% fluid (left-hand side) and a gas water separator (right-hand side) respectively by two valve-controlled tubes. Before filling, the valve connected to the fluid container should be closed previously while the other valve remained opening. Then, a suction pump was turned on to vacuum the inner chamber of the damper and the gas water separator. Afterwards, the closed valve was opened to perfuse the PPG3000-R972-6% fluid into the damper under the driving of air pressure. Owing to the viscosity and shear-thickening phenomenon of the fluid, a larger shear strain induced from a high pressure prefusion process increases the difficulty of prefusion and causes much air remained in the chamber which significantly affects the force performance of damper. As a result, the perfusion process should be divided into several steps to guarantee nil air remainder.

3. Damper performance testing

This section documents the experimental setup for the performance tests of the STFD. The experimental results are discussed and summarized as well.

3.1 Experimental setup

The performance tests were conducted in the small-scale structural laboratory (SSL) at National Center for Research on Earthquake Engineering in Taiwan (Chen *et al*. 2020). Fig. 5 illustrates the experimental setup for the performance testing. One end of the STFD was fixed on the reaction frame, which was fixed on the T-slotted reaction floor. The other end of the damper was hinge-connected to the swivel of a dynamic servo-hydraulic actuator manufactured by MTS Systems Corporation. The maximum stroke and force capacity of the actuator were ±127 mm and ±15 kN, respectively. The MTS FlexTest® Controller FT-100 digital controller in the SSL was used for controlling the dynamic actuator. A load cell with a calibrated capacity of ±15 kN was installed to monitor the axial force imposed on the

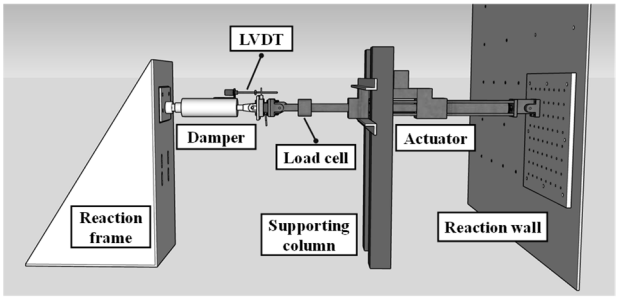

Fig. 5 Illustration of experimental setup for damper performance testing

Table 1 Testing protocol and temperature record of the performance tests

	Testing protocol				Temperature record (°C)	
No.	Amplitude (mm)	Case designation	Frequency (Hz)	Maximum velocity (mm/s)	Initial	Final
1		10 mm-0.1 Hz	0.1	6.28	21.87	21.89
2		10 mm-0.25 Hz	0.25	15.71	21.90	21.92
3		10 mm-0.5 Hz	0.5	31.42	21.89	21.90
4		10 mm-0.75 Hz	0.75	47.12	21.92	21.93
5	10	10 mm-1 Hz	1	62.83	21.93	21.95
6		10 mm-1.5 Hz	1.5	94.25	21.95	21.97
7		10 mm-2 Hz	2	125.66	21.97	22.00
8		10 mm-3 Hz	3	188.50	22.00	22.03
9		10 mm-4 Hz	4	251.33	22.03	22.06
10		20 mm-0.05 Hz	0.05	6.28	22.05	22.08
11		20 mm-0.125 Hz	0.125	15.71	22.05	22.08
12		20 mm-0.25 Hz	0.25	31.42	22.07	22.10
13		20 mm-0.375 Hz	0.375	47.12	22.10	22.14
14	20	20 mm-0.5 Hz	0.5	62.83	22.13	22.16
15		20 mm-0.75 Hz	0.75	94.25	22.16	22.20
16		20 mm-1 Hz	1	125.66	22.19	22.25
17		20 mm-1.5 Hz	1.5	188.50	22.25	22.31
18		20 mm-2 Hz	2	251.33	22.33	22.39
19		25 mm-0.04 Hz	0.04	6.28	22.38	22.41
20		25 mm-0.1 Hz	0.1	15.71	22.40	22.43
21		25 mm-0.2 Hz	0.2	31.42	22.39	22.43
22		25 mm-0.3 Hz	0.3	47.12	22.41	22.46
23	25	25 mm-0.4 Hz	0.4	62.83	22.46	22.50
24		25 mm-0.6 Hz	0.6	94.25	22.50	22.55
25		25 mm-0.8 Hz	0.8	125.66	22.54	22.60
26		25 mm-1.2 Hz	1.2	188.50	22.39	22.47
27		25 mm-1.6 Hz	1.6	251.33	22.51	22.58

damper. A supporting column was used to support part of self-weight of the actuator and damper to prevent the oil-seal of the damper from additional concentrated moment. The actuator was connected to the reaction wall by using four high-tension bolts. A linear variable differential transformer (LVDT) was installed between the fixed cylinder and the moving end of the damper to directly measure the axial displacement of the damper.

3.2 Performance test results

Three equal-amplitude series listed in Table 1 were conducted to realize the performance of the STFD. Each series contained nine sinusoidal excitation frequencies. Seven sinusoidal cycles were performed for each excitation frequency. Accordingly, a total number of 27 tests were carried out for the performance tests of the STFD. It is noted that each series had equally nine levels of maximum velocity. For example, the latest test of each three series possessed an identical maximum velocity of 251.33 mm/sec. However, the excitation frequencies were 4 Hz, 2 Hz, and 1.6 Hz corresponding to series amplitudes of 10 mm, 20 mm, 25 mm, respectively. The test amplitudes and frequencies were reasonably assigned considering the possible range of actual applications.

Displacement-to-force relation of the performance test results were plotted in Fig. 6. Though there were nine tests in each series, merely five selected frequencies of each test series were plotted in Fig. 6 in order to keep the figure from messiness. Meanwhile, since the actuator started from zero and ended at zero velocity in each performance test, the first and last cycles were not considered a complete sinusoidal displacement. Therefore, the test results shown in Fig. 6 and the following analysis ignored the data of the first and last half cycles from the original test records. It is noted that the damper force measured from the experiments was low-pass filtered with a cut-off frequency of 20 times the excitation frequency in each test to remove the measurement noise. The damper displacement was also filtered using the same low-pass filter for data synchronization purpose. As

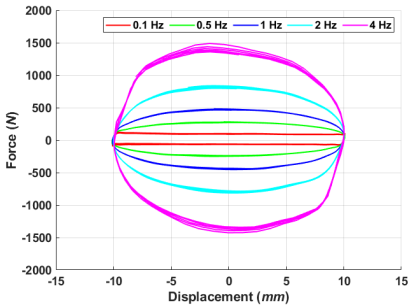

(a) Series with an amplitude of 10 mm

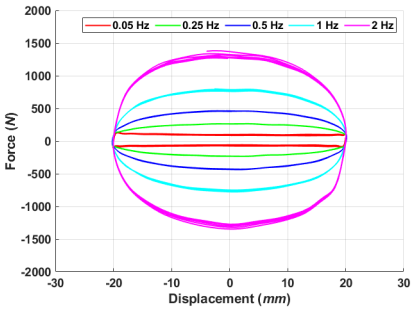

(b) Series with an amplitude of 20 mm

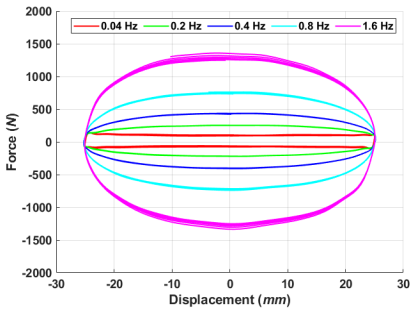

(c) Series with an amplitude of 25 mm

Fig. 6 Displacement-to-force responses of damper performance tests

aforementioned, the STFDs are still in the development phase. Hence, the property of $\alpha > 1$ was obscure and merely existed in a very minor velocity stage which was difficult to be observed in the performance test results. This defect needs to be further solved through the design of damper mechanism in the future. On the other hand, the temperature monitored from the thermocouple at the beginning and the end of each test was recorded as shown in Table 1, in which the initial temperature of each test remained 22°C approximately. Obviously, the increase of temperature was limited during the tests. However, there was slight difference on the temperature rise among the tests due to the accumulative energy that was dissipated in each test.

4. Numerical model of shear-thickening fluid damper

4.1 Discrete-time Bouc-Wen model

The discrete Bouc-Wen model derived by Crivellaro and Donha (2008) aimed at discretizing an MR damper model

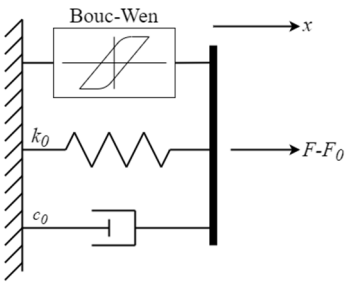

Fig. 7 Schematic of the modified Bouc-Wen model

proposed by Spencer *et al*. (1997). The differential equation was modified to a difference equation by approximating the state derivative with a difference using a backward difference method which resulted in a stable discrete-time system. In this study, a modified Bouc-Wen model was first utilized to simulate the behavior of the STFD as depicted in Fig. 7. The equations of the damper model are given by

$$z[k] = \frac{A\dot{x}[k]\Delta t + z[k-1]}{\xi + \gamma|\dot{x}[k]||z[k-1]|\Delta t + \beta\dot{x}[k]z[k-1]\Delta t} \tag{2}$$

$$F[k] = c_0\dot{x}[k] + k_0x[k] + \lambda z[k] + F_0 \tag{3}$$

where z is the evolutionary variable used in the Bouc-Wen hysteretic model in the unit of displacement; x and $\dot{x}$ are the damper displacement and velocity, respectively; F_0, c_0, and k_0 are the parameters to accommodate to initial damper force, damping coefficient, and stiffness, correspondingly; A, ξ, γ, β, and λ are the discrete-time Bouc-Wen model parameters that control the linearity in the unloading and the smoothness of the transition from the pre-yield to the post-yield region; and k and Δt represent the time step and time increment, individually. Accordingly, the discrete-time model has 8 parameters to be adjusted for simulating the behavior of the STFD.

4.2 Symbiotic organisms search (SOS)

The parameters of the damper model were optimized by applying a novel metaheuristic optimization method named symbiotic organisms search (SOS) (Cheng and Prayogo 2014). The algorithm simulates the reliance behavior of one organism on other species known as symbiosis. Three common symbioses are used in the SOS algorithm including the mutualism phase, commensalism phase, and parasitism phase. The flowchart of SOS is illustrated in Fig. 8. The SOS starts the initialization by assigning a pre-determined number of organisms with random position in the n^{th} dimensional search space in which n represents the number of parameters to be optimized. The fitness value of each organism is obtained based on a user-defined objective function. The position of the organism that has the best fitness value is memorized as $\mathbf{x}_{\text{best}}$. In the mutualism phase, two organisms are randomly selected. The position of each organism is then updated by using the equation defined as

$$\boldsymbol{x}_{\boldsymbol{inew}} = \boldsymbol{x}_{\boldsymbol{i}} + rand(0,1) \cdot \left(\boldsymbol{x}_{\boldsymbol{best}} - \frac{\boldsymbol{x}_{\boldsymbol{i}} + \boldsymbol{x}_{\boldsymbol{j}}}{2} \cdot BF_1\right) \tag{4}$$

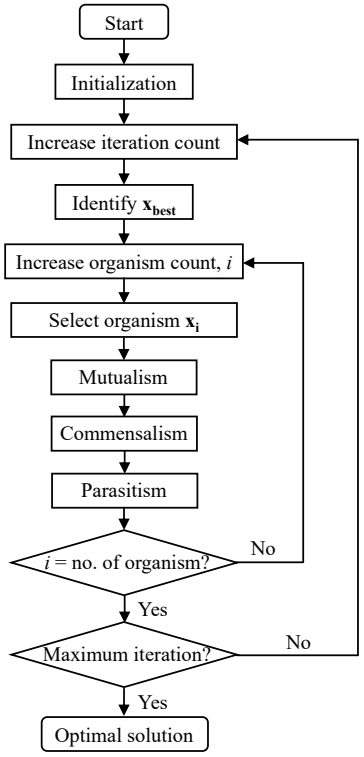

Fig. 8 Flowchart of symbiotic organisms search

$$\boldsymbol{x_{jnew}} = \boldsymbol{x_j} + rand(0,1) \cdot \left(\boldsymbol{x_{best}} - \frac{\boldsymbol{x_i} + \boldsymbol{x_j}}{2} \cdot BF_2\right) \quad (5)$$

where $\mathbf{x}_{inew}$ and $\mathbf{x}_{jnew}$ are the new position of the i^{th} and j^{th} organisms; and BF_1 and BF_2 are benefit factors of the i^{th} and j^{th} organisms, respectively. Since BF_1 and BF_2 represent the benefit level to individual organism, they are randomly determined as either 1 or 2 at each iteration step. In the SOS, the new position of the selected organism is evaluated by calculating its fitness value. If the fitness value of the new position is better than that of the previous position, then the position is updated by the new position of the organism. Otherwise, the original position is retained.

In the commensalism phase, the position of the selected organism is updated by using the equation defined as

$$\boldsymbol{x_{inew}} = \boldsymbol{x_i} + rand(-1,1) \cdot (\boldsymbol{x_{best}} - \boldsymbol{x_j}) \quad (6)$$

From Eq. (6), it can be seen that the i^{th} organism intends to get benefit from the j^{th} organism. If the fitness value evaluated by the new position is better than the previous one, then the position is updated by the new position of the organism. Otherwise, the original position is sustained. In the parasitism phase, a new parasite vector is created by duplicating a randomly-selected organism with modified parameters which are also selected arbitrarily. Then another randomly-selected organism serves as the host to be parasitized by the parasite. Both the two organisms (parasite and host) are then evaluated by their fitness values. If the parasite has a better fitness value than the host, the host organism is dead and replaced by the parasite in the ecosystem. On the contrary, if the fitness value of the parasite is inferior to that of the host, the parasite is vanished immediately in the ecosystem. The processes of the mutualism phase, commensalism phase, and parasitism phase are repeated until all the organisms in the ecosystem have been selected as $\mathbf{x}_i$. The entire process is repeated until the user-defined stopping criterion is reached which can be set as iteration numbers or required performance.

4.3 Optimization results

The discrete-time damper model composed of a Bouc-Wen model, a spring, and a dashpot was used to simulate the response of the STFD. It was realized that there were 8 parameters to be optimized by applying the SOS algorithm as shown in Eqs. (2) and (3). At the early stage of this study, it remained unknown if the discrete-time damper model was able to simulate the response of the STFD. Thus, the normalized root-mean-square error (NRMSE) between the damper force obtained from the experimental data and from the discrete-time damper model was adopted as the objective function in the beginning which can be expressed as

$$\text{NRMSE}(\%) = \sqrt{\frac{\sum_{k=1}^{N}(F_e[k] - F_m[k])^2}{\sum_{k=1}^{N} F_e[k]^2}} \times 100\% \quad (7)$$

where $F_e[k]$ and $F_m[k]$ are the damper force obtained from the experiment and numerical model at the k^{th} step, respectively; and N is the number of data points. It is realized that better model parameters lead to a smaller NRMSE. Noted that a total of 8 parameters needed to be identified. The first step was focused on the feasibility of the damper model. The experimental data with sinusoidal displacement with an amplitude of 20 mm and a frequency of 0.125 Hz (denoted as 20 mm-0.125 Hz) were used for optimizing the 8 parameters of the discrete-time damper model. In the optimization process, 200 organisms were adopted and 1000 iterations were determined as the stopping criterion. A total number of 20 optimization trials were conducted in order to evaluate the consistency of the obtained optimal parameters. During the optimization in the beginning, it was found that all the trials converged to a constant within 500 iterations. Therefore, 1000 iterations were considered sufficient enough for each trial to converge to an optimal value for all the optimization in this study. Table 2 lists the 8 optimal parameters of each trial. It can be observed that the optimal parameters obtained from each trial are different, especially for A, λ, and γ. On the contrary, the parameters ξ, c_0, k_0, and F_0 are mostly identical from each trial which indicates that the damper response of the Bouc-Wen model is mostly dominated by these parameters. The other parameters are less sensitive to the damper response. However, the final NRMSE of each trial converges to an identical value of 3.6383% with a standard variation of 1.315×10^{-6}%. In other words, there are multiple optimal points that achieved the identical minimum value of the objective function. The optimization results demonstrated that the minimum NRMSE could be resulted from various parameter sets of the damper model. Fig. 9 shows the damper responses from both the experiment and

Table 2 Optimal damper parameters and NRMSE using experimental data of 20 mm-0.125 Hz

Trial no.	A	λ (N/mm)	β (1/mm^2)	γ (1/mm^2)	ξ	c_0 (N-s/mm)	k_0 (N/mm)	F_0 (N)	NRMSE (%)
1	0.7730	599.9301	0.0000	43.6209	1.0023	3.9103	0.0000	16.3198	3.6383
2	1.0738	431.8745	0.0000	31.4011	1.0023	3.9103	0.0000	16.3197	3.6383
3	1.0859	427.0692	0.0000	31.0539	1.0023	3.9104	0.0000	16.3188	3.6383
4	1.5256	303.9682	0.0000	22.1018	1.0023	3.9104	0.0000	16.3200	3.6383
5	1.6157	287.0231	0.0000	20.8698	1.0023	3.9104	0.0000	16.3200	3.6383
6	1.9158	242.0370	0.0000	17.5965	1.0023	3.9102	0.0000	16.3208	3.6383
7	2.1204	218.7232	0.0000	15.8986	1.0024	3.9092	0.0000	16.3197	3.6383
8	2.1550	215.1963	0.0000	15.6469	1.0023	3.9103	0.0000	16.3198	3.6383
9	2.3987	193.3244	0.0000	14.0561	1.0023	3.9102	0.0000	16.3195	3.6383
10	2.4262	191.1375	0.0000	13.8975	1.0023	3.9104	0.0000	16.3200	3.6383
11	2.5504	181.8264	0.0000	13.2212	1.0023	3.9105	0.0000	16.3197	3.6383
12	2.8435	163.0856	0.0000	11.8578	1.0023	3.9103	0.0000	16.3200	3.6383
13	3.7259	124.4649	0.0000	9.0506	1.0023	3.9104	0.0000	16.3198	3.6383
14	4.6132	100.5284	0.0000	7.3101	1.0023	3.9104	0.0000	16.3195	3.6383
15	8.5114	54.4879	0.0000	3.9621	1.0023	3.9103	0.0000	16.3197	3.6383
16	8.6365	53.7013	0.0000	3.9048	1.0023	3.9100	0.0000	16.3180	3.6383
17	21.1744	21.9051	0.0000	1.5939	1.0023	3.9116	0.0000	16.3224	3.6383
18	22.1889	20.8993	0.0000	1.5196	1.0023	3.9103	0.0000	16.3200	3.6383
19	73.5974	6.3004	0.0000	0.4580	1.0023	3.9103	0.0000	16.3181	3.6383
20	118.4979	3.9125	0.0000	0.2845	1.0023	3.9111	0.0000	16.3178	3.6383

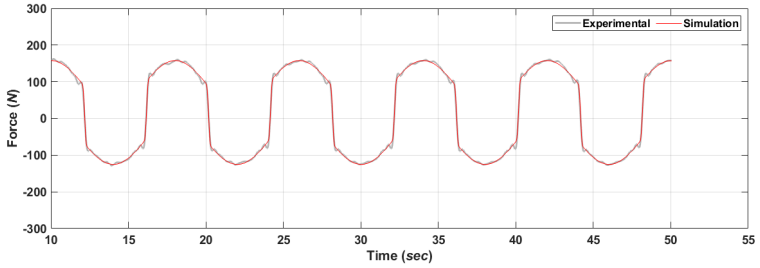

(a) Force time history

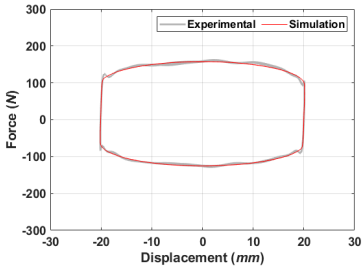

(b) Displacement-to-force hysteresis loop

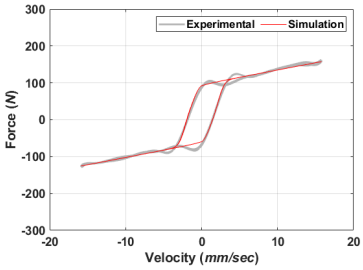

(c) Velocity-to-force hysteresis loop

Fig. 9 Damper responses from performance test and numerical simulation (20 mm-0.125 Hz)

numerical model with the parameter set of the first trial in Table 2. The results indicate that the damper model can simulate the damper response regarding the force time history, displacement-to-force relationship, and velocity-to-force relationship. However, the response of the damper model with the same set of parameters could be different from the experimental result when the damper was subjected to the same sinusoidal amplitude with larger frequency. Fig. 10 reveals the damper responses from the experiment and numerical model subjected to sinusoidal displacement with an amplitude of 20 mm and a frequency of 2 Hz (denoted as 20 mm-2 Hz). It can be clearly seen that the set of parameters of the damper model optimized by the experimental data of the case 20 mm-0.125 Hz cannot

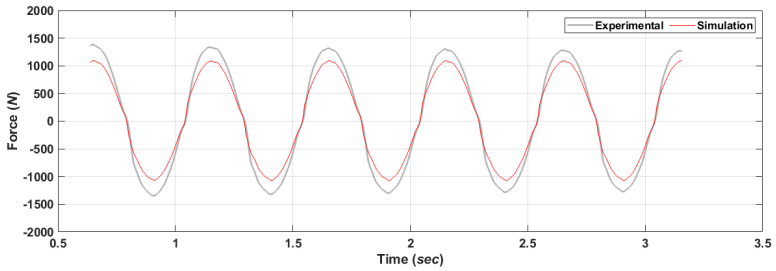

(a) Force time history

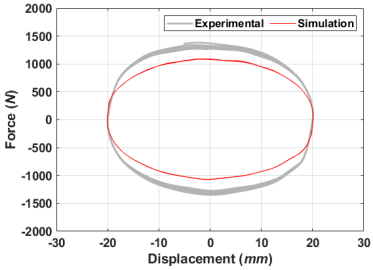

(b) Displacement-to-force hysteresis loop

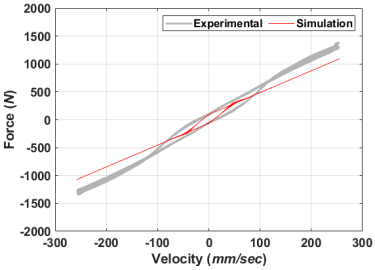

(c) Velocity-to-force hysteresis loop

Fig. 10 Damper responses from performance test and numerical simulation (20 mm-2 Hz)

Table 3 Optimal damper parameters and RMS using all experimental data with a fixed amplitude of 20 mm

Trial no.	A	λ (N/mm)	β (1/mm^2)	γ (1/mm^2)	ξ	c_0 (N-s/mm)	k_0 (N/mm)	F_0 (N)	NRMSE (%)
1	1.1227	456.5833	0.0000	57.8855	0.9914	5.5275	0.0043	15.1465	8.9883
2	1.6722	306.5527	0.0000	38.8645	0.9914	5.5275	0.0043	15.1466	8.9883
3	1.7038	300.8624	0.0000	38.1435	0.9914	5.5275	0.0043	15.1473	8.9883
4	2.5807	198.6417	0.0000	25.1855	0.9914	5.5275	0.0043	15.1451	8.9883
5	2.7931	183.5337	0.0000	23.2683	0.9914	5.5275	0.0043	15.1462	8.9883
6	3.1167	164.4811	0.0000	20.8533	0.9914	5.5275	0.0043	15.1464	8.9883
7	3.4384	149.0865	0.0000	18.9010	0.9914	5.5275	0.0043	15.1465	8.9883
8	3.4508	148.5537	0.0000	18.8341	0.9914	5.5275	0.0043	15.1468	8.9883
9	3.6359	140.9902	0.0000	17.8747	0.9914	5.5275	0.0043	15.1463	8.9883
10	5.7878	88.5701	0.0000	11.2290	0.9914	5.5275	0.0043	15.1464	8.9883
11	6.2482	82.0460	0.0000	10.4017	0.9914	5.5274	0.0042	15.1479	8.9883
12	6.6960	76.5555	0.0000	9.7055	0.9914	5.5275	0.0043	15.1465	8.9883
13	6.7589	75.8437	0.0000	9.6156	0.9914	5.5275	0.0043	15.1466	8.9883
14	7.3008	70.2134	0.0000	8.9014	0.9914	5.5275	0.0043	15.1464	8.9883
15	10.3913	49.3325	0.0000	6.2543	0.9914	5.5275	0.0043	15.1463	8.9883
16	10.7969	47.4720	0.0000	6.0176	0.9914	5.5275	0.0043	15.1463	8.9883
17	14.8773	34.4633	0.0000	4.3697	0.9914	5.5275	0.0043	15.1459	8.9883
18	15.4976	33.0743	0.0000	4.1928	0.9914	5.5275	0.0042	15.1473	8.9883
19	16.6266	30.8325	0.0000	3.9090	0.9914	5.5275	0.0043	15.1466	8.9883
20	28.2102	18.1704	0.0000	2.3035	0.9914	5.5275	0.0044	15.1453	8.9883

represent the damper behavior of the case 20 mm-2 Hz. The NMRSE increases to 19.5388%. It demonstrates that optimization of the parameters cannot merely consider one experimental data since the behavior of the STFD varies at different velocity levels.

In order to obtain a set of parameters for the damper model which were optimized by applying numerous experimental data sets, the objective function was then changed into the root-mean-square (RMS) of the NRMSE of each experimental data which can be expressed as

$$\mathrm{RMS}(\%) = \sqrt{\frac{\sum_{k=1}^{N_e} \mathrm{NRMSE}_k{}^2}{N_e}} \times 100\% \quad (8)$$

where N_e is the number of experiments adopted for the parameter optimization. By applying the SOS algorithm with identical number of organisms and iterations (200 organisms and 1000 iterations) and considering all the 9 experimental data sets with an amplitude of 20 mm, the optimal parameters of the damper model were obtained. Similarly, a total number of 20 optimization trials were conducted in order to evaluate the consistency of the obtained optimal parameters. Table 3 lists the optimized parameters of the damper model from each trial. The results show similar tendency as the previous results. All the 20 trials converge to the same RMS values; however, the model parameters vary in different trials. The final RMS of each trial converges to 8.9883% with a standard variation of 7.9239×10^{-8}%. Figs. 11 and 12 show the damper responses obtained from both the experiment and numerical model for the case of 20 mm-0.125 Hz and 20 mm-2 Hz, respectively in which the damper model parameters of the first trial

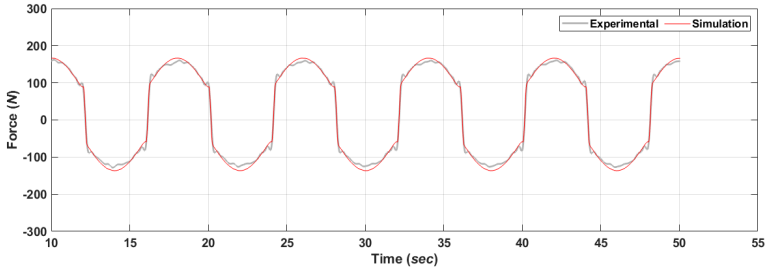

(a) Force time history

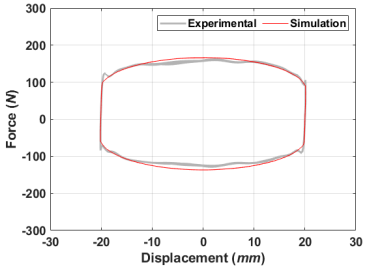

(b) Displacement-to-force hysteresis loop

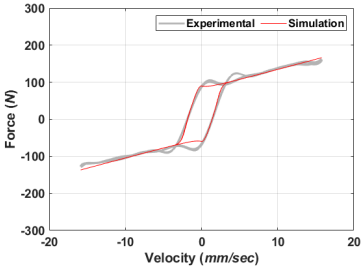

(c) Velocity-to-force hysteresis loop

Fig. 11 Damper responses from performance test and numerical simulation with parameters optimized by RMS (case 20 mm-0.125 Hz)

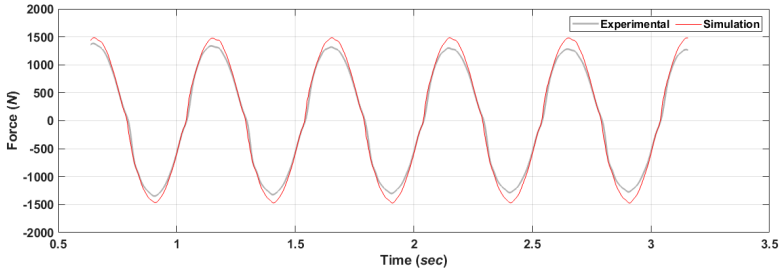

(a) Force time history

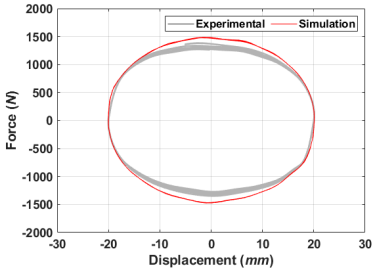

(b) Displacement-to-force hysteresis loop

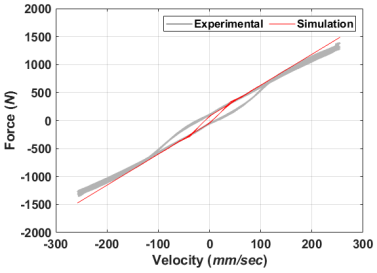

(c) Velocity-to-force hysteresis loop

Fig. 12 Damper responses from performance test and numerical simulation with parameters optimized by RMS (case 20 mm-2 Hz)

listed in Table 3 were selected. The results indicate that the damper model simulates the damper response with an NRMSE of 6.5565% and 11.1904% corresponding to the case of 20 mm-0.125 Hz and 20 mm-2 Hz, respectively. Since the damper parameters were optimized based on the overall performance of sinusoidal tests with a fixed amplitude of 20 mm, the NRMSE becomes larger in the case of 20 mm-0.125 Hz and smaller in the case of 20 mm-2 Hz compared to the previous results with the damper parameters optimized by considering merely the data of 20 mm-0.125 Hz. In other words, the damper model with the parameters optimized by minimizing the objective function of RMS (Eq. (8)) achieves balanced performance among all the experimental data sets with a fixed amplitude of 20 mm. This means that damper model performance gets improved by using more experimental data with different frequencies. Nevertheless, when the damper is subjected to a maximum velocity above 200 mm/sec, the performance of the damper model on modelling the velocity-to-force hysteresis loop is not accurate enough with the velocity lower than 100 mm/sec as shown in Fig. 12(c). Therefore, the numerical model of the STFD needs to be further modified in order to simulate damper response accurately with a broadband velocity range.

5. Numerical model with transit parameters

A two-stage numerical model with transit sets of parameters was proposed by modifying the previous model in order to accommodate the varying behaviour of the STFD from low velocity to high velocity.

5.1 Optimization of transit parameters

The velocity for transiting the two sets of parameters, denoted as V_L is crucial to the performance of the damper model; therefore, it is necessary to consider V_L as one of the parameters to be optimized. However, since the two sets of parameters may be significantly different from each other, a sudden change of damper force could be occurred around the velocity V_L, leading to a discontinuity of damper force when the parameters are transited from one set to the other set. Consequently, a continuous function that can smoothly switches between two values at a defined point is essential such as the sigmoid function and the hyperbolic tangent function. In this study, the sigmoid function with a s-shaped curve was adopted for smoothly transiting the parameter sets which can be expressed as

$$S(x) = \frac{1}{1 + e^{-x}} \tag{9}$$

It is obvious that the minimum and maximum return values of the sigmoid function are 0 and 1, respectively. The smoothly switching of value from 0 to 1 is used to represent that either the 1st or the 2nd set of parameters is adopted for the damper model, correspondingly. When the return value is between 0 to 1, it indicates that transit parameters between the two sets of parameters are applied to the damper model. A second parameter V_R that represents the transition range of velocity in the sigmoid function for the damper model is also important to the damper model performance and treated as a parameter to be optimized as well. It is noted that the return value of the sigmoid function (Eq. (9)) starts to increase from 0 at x = -10, increases dramatically at x = 0, and approximates to 1 at x = 10. Therefore, the range from x = -10 to x = 10 was adopted for the normalization of the sigmoid function related to V_L and V_R. Accordingly, the transition range for the damper velocity ($V_L \pm V_R$) needs to be normalized to the range from -10 to 10 in the sigmoid function. The modified sigmoid function adopted in this study can be expressed as

$$S[k] = \frac{1}{1 + e^{-\bar{x}[k]}} \quad \text{where} \quad \bar{x}[k] = \frac{\dot{x}[k] - V_L}{V_R} \times 10 \tag{10}$$

Noted that there are 8 parameters in one parameter set including A, λ, β, γ, ξ, c_0, k_0, and F_0. Let the two parameter sets become two row vectors $\mathbf{P}_1$ and $\mathbf{P}_2$ in which $\mathbf{P}_1 = [A_1\ \lambda_1\ \beta_1\ \gamma_1\ \xi_1\ c_{01}\ k_{01}\ F_{01}]$ and $\mathbf{P}_2 = [A_2\ \lambda_2\ \beta_2\ \gamma_2\ \xi_2\ c_{02}\ k_{02}\ F_{02}]$, the parameter set $\mathbf{P}$ adopted in the damper model becomes velocity-dependent and varies step-by-step as

$$\boldsymbol{P}[k] = S[k](\boldsymbol{P}_2 - \boldsymbol{P}_1) + \boldsymbol{P}_1 \tag{11}$$

Fig. 13 illustrates the transition of parameter sets based on Eq. (11). If the damper velocity is smaller than V_L-V_R, the parameters adopted for the damper model are in $\mathbf{P}_1$. Similarly, if the damper velocity is larger than V_L+V_R, the parameters adopted for the damper model are in $\mathbf{P}_2$. Lastly, if the damper velocity is between V_L-V_R and V_L+V_R, the transition of parameters follows Eq. (11).

There were a total number of 18 parameters to be optimized for the modified numerical damper model with transit parameters including the two parameter sets $\mathbf{P}_1$ and $\mathbf{P}_2$ as well as V_L and V_R. The modified damper model was optimized using SOS with 200 organisms and 1000 iterations. Similar to the previous procedure, 20 optimization trials were conducted in order to evaluate the consistency of the optimal parameters. All the 9 experimental data sets with an amplitude of 20 mm were used for the parameter optimization with the objective function identical to the previous optimization as defined in Eq. (8). The optimized parameters of the 20 trials for the 1st set ($\mathbf{P}_1$) and the 2nd set ($\mathbf{P}_2$) are listed in Tables 4 and 5, respectively. Note that the two parameter sets $\mathbf{P}_1$ and $\mathbf{P}_2$

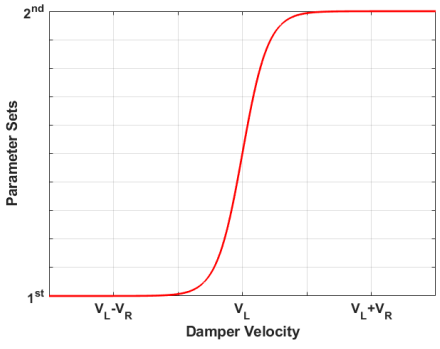

Fig. 13 Illustration of transition of parameter set for the damper model

Table 4 Optimal damper parameters of the 1st set using all experimental data with a fixed amplitude of 20 mm from 20 trials

Trial no.	A_1	λ_1 (N/mm)	β_1 (1/mm^2)	γ_1 (1/mm^2)	ξ_1	c_{01} (N-s/mm)	k_{01} (N/mm)	F_{01} (N)
1	2.4508	371.2524	0.0002	0.0026	0.8523	5.9839	0.0000	4.9077
2	16.4979	56.2054	0.0000	0.0000	0.8518	6.1964	0.0009	5.2285
3	4.4635	201.9838	0.0000	0.0001	0.8494	4.9189	0.0000	4.7973
4	5.4655	165.6524	0.0003	0.0002	0.8491	5.0453	0.0000	4.8402
5	35.6279	25.2313	0.0000	0.0005	0.8526	5.3546	0.0000	5.1230
6	2.9373	308.5300	0.0125	0.0000	0.8504	5.2710	0.0000	4.3726
7	5.3351	175.6043	0.0000	0.0011	0.8502	5.8027	0.0001	5.4416
8	29.9185	30.9576	0.0358	0.0003	0.8495	5.5954	0.0000	4.9975
9	9.2857	96.4134	0.0077	0.0025	0.8483	2.8657	0.0000	4.7546
10	7.1830	118.9510	0.0001	0.0012	0.8427	0.0319	0.0004	5.0380
11	99.6984	8.6068	0.0001	0.0000	0.8462	0.1199	0.0002	6.0439
12	9.9862	106.3017	0.0087	0.0000	0.8460	10.1304	0.0000	7.7629
13	11.0906	51.0234	0.0000	0.0253	0.8488	0.0000	0.0000	4.4482
14	9.6650	72.2679	0.6930	6.2970	1.0062	2.1452	1.3948	11.4600
15	0.0000	0.0000	0.0000	0.0000	1.0654	64.0414	4.5353	11.5975
16	0.0000	0.0000	0.0000	0.0000	1.0654	64.0414	4.5353	11.5975
17	333.5892	600.0000	133.7522	212.2620	1.1394	27.3819	73.9058	-158.9749
18	0.0000	220.7480	0.0000	0.0804	5.0000	100.0000	7.6247	3.9298
19	0.0000	0.0000	299.6498	0.0000	1.0255	71.1164	4.5475	10.8748
20	0.0000	0.0000	534.3157	0.0000	1.0250	71.4204	4.5494	10.8758

Table 5 Optimal damper parameters of the 2nd set using all experimental data with a fixed amplitude of 20 mm from 20 trials

Trial no.	A_2	λ_2 (N/mm)	β_2 (1/mm^2)	γ_2 (1/mm^2)	ξ_2	c_{02} (N-s/mm)	k_{02} (N/mm)	F_{02} (N)
1	0.2695	599.9977	2.5578	0.1238	1.1464	4.6397	0.0000	16.5783
2	1.8521	87.1116	0.1653	0.2183	1.1470	4.6351	0.0000	16.6089
3	0.4930	330.1373	0.0018	1.4379	1.1489	4.6247	0.0000	16.6102
4	0.6064	269.0898	0.0078	1.1650	1.1492	4.6229	0.0000	16.5904
5	4.0471	40.3847	0.0003	0.1757	1.1496	4.6221	0.0000	16.5872
6	0.3249	498.0157	0.0243	2.1269	1.1482	4.6232	0.0000	16.6930
7	0.6104	266.0437	0.0019	1.1592	1.1482	4.6205	0.0000	16.5031
8	3.3246	48.8341	0.0000	0.2129	1.1489	4.6279	0.0004	16.5515
9	0.9950	166.1896	0.7421	0.0000	1.1509	4.6287	0.0098	16.7026
10	0.7633	220.3909	0.0566	0.8694	1.1561	4.5924	0.0003	16.5131
11	10.5799	15.9058	0.0152	0.0580	1.1531	4.6319	0.0017	16.3337
12	1.5974	108.4435	0.3910	0.0958	1.1635	4.6198	0.0008	15.9096
13	0.8929	181.8772	0.2143	0.5666	1.1484	4.6220	0.0033	16.4171
14	1.8853	132.7097	0.0111	9.8980	0.9807	5.6367	0.0005	15.3649
15	0.8948	302.5511	0.0000	25.0576	0.9757	5.6266	0.0000	15.2805
16	5.2227	51.8338	0.0000	4.2929	0.9757	5.6266	0.0000	15.2805
17	4.2019	121.9993	0.0000	15.4671	0.9914	5.5275	0.0043	15.1465
18	231.7072	7.4544	0.0119	1.6077	1.6389	5.2879	0.0008	15.5915
19	46.2519	161.0653	119.4680	228.4724	0.6759	5.6032	0.0384	15.3997
20	26.2808	283.9865	210.1047	403.4774	0.6799	5.6025	0.0386	15.3998

Table 6 Optimal parameters for the sigmoid function using all experimental data with a fixed amplitude of 20 mm from 20 trials

Trial no.	V_L (mm/s)	V_R (mm/s)	RMS (%)
1	0.0026	25.0155	5.1749
2	0.0085	25.1252	5.1777
3	0.0002	25.4242	5.1791
4	0.0016	25.4317	5.1791
5	0.0659	25.3527	5.1793
6	0.0043	25.3689	5.1794
7	0.0000	25.4940	5.1803
8	0.0022	25.3462	5.1821
9	0.0066	25.4960	5.1857
10	0.0009	26.4667	5.1878
11	0.0047	26.0240	5.1900
12	0.1938	27.0667	5.2119
13	0.0003	23.7925	5.2303
14	1.2773	1.0186	8.3141
15	0.5632	0.9600	8.3422
16	0.5632	0.9600	8.3422
17	0.0000	0.0000	8.9883
18	0.0004	9.1163	9.9521
19	0.7495	2.2525	10.0753
20	0.7490	2.2529	10.0753

were optimized simultaneously to accommodate to the varying behaviour of the STFD from low velocity to high velocity. Therefore, it was expected to obtain two different parameter sets $\mathbf{P}_1$ and $\mathbf{P}_2$ from the same trial which can be clearly seen in Tables 4 and 5. Table 6 shows for the optimal parameters of the normalized sigmoid function for transition of parameter sets. The parameters of each trial are listed from the smallest value to the largest value of the objective function (RMS) in the three tables. It can be found from Table 6 that merely the first 12 trials have similar RMS values among which the smallest is 5.1749%. The RMS values of the rest 8 trials are significantly larger than 5.1749%. Unlike the RMS value of each trial which converges to a consistent optimal value for the damper model with single parameter set, the standard deviation of RMS of the 20 trials is 2.0004% which indicates that the SOS may not permanently achieve optimal solution for the damper model with transit parameters.

The 18 parameters which resulted in the smallest RMS value (the first row in Tables 4, 5, and 6) were adopted for the damper model with transit parameters for the following discussions. The parameters were treated as the global optimum which provided the optimal solution among all the 20 trials. Figs. 14 and 15 show the damper responses obtained from both the experiment and damper model with transit parameters for the case of 20 mm-0.125 Hz and 20 mm-2 Hz, respectively. The results indicate that the damper model simulates the damper response with an NRMSE of 4.3418% and 7.9398%, respectively corresponding to the case of 20 mm-0.125 Hz and 20 mm-2 Hz, respectively. It is apparent that the damper model with transit parameter sets simulates the damper response better than that with merely single parameter set in both two cases. It can be clearly seen by comparing Figs. 11(c) and 14(c) as well as Figs. 12(c) and 15(c) that the damper model with transit parameter sets achieves more accurate velocity-to-force hysteresis loop than the model with single parameter set. The RMSEs between the experimental response and the simulation results obtained from the damper model with single parameter set and with transit parameter sets are shown in Table 7. It can be found that the damper model with transit parameter sets have smaller NRMSE than that with single parameter set for most cases. The average NRMSE of the damper model with single parameter set and transit parameter sets are 8.3123% and 5.4869%, respectively, which demonstrates that the damper model with the

Table 7 Comparison of damper model performance with single parameter set and transit parameter sets

No.	Amplitude (mm)	Frequency (Hz)	NRMSE of the model with single parameter set (%)	NRMSE of the model with transit parameter sets (%)
1		0.1	10.3795	4.9720
2		0.25	7.6863	5.4466
3		0.5	7.9326	5.6767
4		0.75	9.2916	5.3312
5	10	1.0	9.8862	3.4500
6		1.5	9.4912	2.5708
7		2.0	7.7992	3.8960
8		3.0	6.1038	7.1836
9		4.0	18.3976	13.1168
10		0.05	11.1904	4.3418
11		0.125	5.9090	2.4985
12		0.25	4.5110	2.9409
13		0.375	6.3595	3.0719
14	20	0.5	7.6510	1.9223
15		0.75	7.3936	2.0151
16		1.0	4.0726	5.1628
17		1.5	6.5565	7.9398
18		2.0	18.2589	10.0193
19		0.04	12.3935	5.8772
20		0.1	7.0254	3.5777
21		0.2	4.1718	4.0552
22		0.3	3.3467	3.9281
23	25	0.4	3.8699	5.2595
24		0.6	3.7292	6.5051
25		0.8	3.3167	7.7242
26		1.2	8.8407	9.7395
27		1.6	18.8684	9.9243
Average			8.3123	5.4869

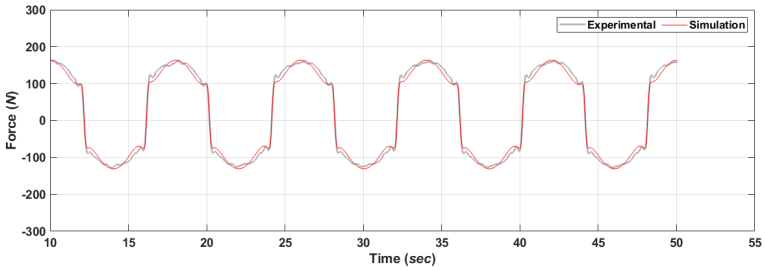

(a) Force time history

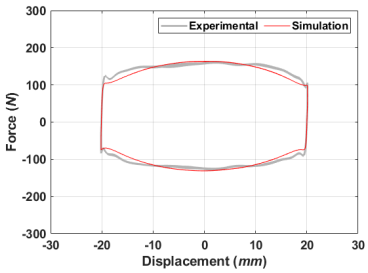

(b) Displacement-to-force hysteresis loop

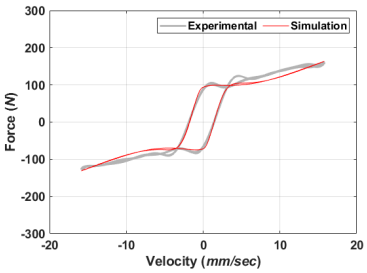

(c) Velocity-to-force hysteresis loop

Fig. 14 Damper responses from performance test and numerical simulation with transit parameters optimized by RMS (case 20 mm-0.125 Hz)

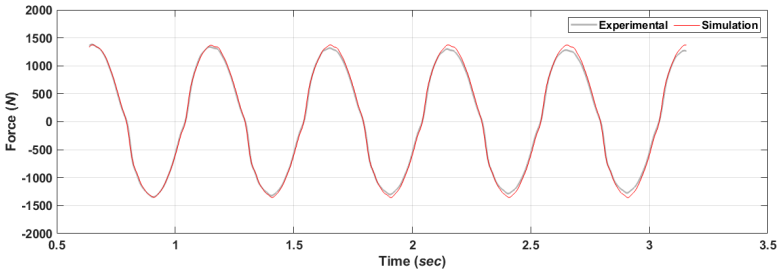

(a) Force time history

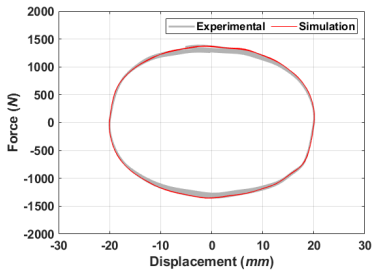

(b) Displacement-to-force hysteresis loop

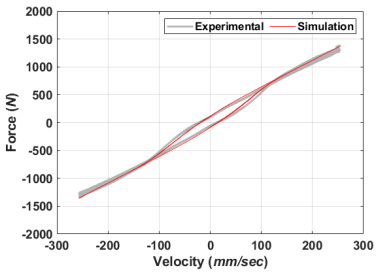

(c) Velocity-to-force hysteresis loop

Fig. 15 Damper responses from performance test and numerical simulation with transit parameters optimized by RMS (case 20 mm-2 Hz)

proposed optimal transit parameter sets improves the modelling accuracy on the behavior of the STFD.

5.2 Performance under random excitation

After the damper model with transit parameters were optimized, additional two damper tests were conducted for further verifying the damper model performance. Two band-limited white noise displacement time histories with a bandwidth from 0 Hz to 20 Hz, and a duration of 30 seconds were used as the input to the STFD. The maximum velocity of the two random excitations are 165 mm/s and 200 mm/s, respectively. Fig. 16 shows the damper responses under one of the two random excitations from the experiments as well as from the damper model with single parameter set and with transit parameter sets. It can be clearly seen that the modified damper model with transit parameters simulates the STFD much better than the discrete Bouc-Wen model does regarding both the displacement-to-force and the velocity-to-force relationships. The NRMSEs of the damper response under the two random excitations between the experimental and the simulation results of the discrete Bouc-Wen model with single parameter set are 27.7094% and 28.1798%.

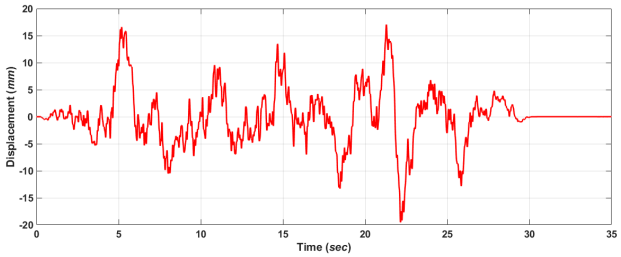

(a) Random displacement time history

(b) Simulation result of the damper model with single parameter set

(c) Simulation result of the damper model with transit parameter sets

Fig. 16 Damper responses from experiment and numerical simulation under random excitation

However, the NRMSEs are reduced to 15.6541% and 15.8974% if the damper model is replaced by the one with transit parameters. It demonstrates that the proposed two-stage damper model with transit sets of parameters accommodates the varying behavior of the STFD from low velocity to high velocity much better than the conventional discrete Bouc-Wen model. This modified damper model can be incorporated into structural analysis of a seismically isolated building for future studies.

6. Conclusions

A representative numerical damper model for simulating dynamic response of the shear-thickening fluid damper (STFD) is required for analyses of structures in which the STFDs are installed. In this study, a STFD has been designed, fabricated, and installed in the laboratory. A series of harmonic performance tests were conducted which contained three amplitude levels. Nine cyclic frequencies were varied for each amplitude level, leading to a total number of 27 performance test cases for the damper. A modified discrete-time Bouc-Wen model which contained 8 parameters was first adopted to simulate the responses of the STFD. A novel metaheuristic optimization algorithm named symbiosis organisms search (SOS) was applied to optimize the 8 parameters of the damper model as the SOS needed not to tune any parameter in prior before conducting the optimization. The normalized root-mean-square error (NRMSE) between the damper force from the tests and the damper model was selected as the objective function in the beginning. The optimization results indicate that the damper model parameters optimized by the experimental data of one test case cannot represent the damper response of another test case especially when the maximum velocity in the two cases was significantly different. Due to the varying response of the STFD from low velocity to high velocity, it is difficult to optimize the damper model parameters by merely considering the experimental data with nearby maximum velocity. Afterwards, the root-mean-square (RMS) of the NRMSE of each experimental data was adopted as the objective function in order to obtain an optimal set of parameters for the damper model considering the experimental data with a broad range of maximum velocity. Simulation results of the damper model were improved; however, further improvement was required within the velocity lower than 100 mm/sec.

In this study, a two-stage discrete Bouc-Wen model with optimal transit sets of parameters has been proposed and verified. One parameter set of the discrete Bouc-Wen model was transited to the other parameter set through the proposed parameter transition function. The transition function, which was modified from the sigmoid function considered the critical transition velocity and the velocity

range for smooth transition. As a result, a total number of 18 parameters needed to be optimized for the damper model with transit parameters. Numerical simulation results indicated that the damper model with transit parameters outperformed that with merely single parameter set for the 27 performance tests under sinusoidal excitations. Averagely speaking, the NRMSE was reduced from 8.3123% to 5.4869% which was 33.99% improvement on the simulation accuracy of the damper model. Finally, two damper tests with random excitations were adopted to further verify the simulation performance of the proposed damper model. Numerical simulation results demonstrated that the damper model with transit parameters accommodated the varying behavior of the STFD from low velocity to high velocity well, providing an optimal and stable damper model for structural analyses of a seismically isolated building. Considering that there are some parameters in the Bouc-Wen model which are less sensitive to the damper response, a simplified model with fewer but more significant parameters should be developed and applied to the transition method for the shear-thickening fluid damper in the future.

Acknowledgments

The authors would like to express our sincere gratitude to the experimental facilities and expense supported by NCREE (06110A2500) as well as the financial support provided by the Ministry of Science and Technology, Republic of China (Taiwan) (MOST 108-2221-E-011-006-MY2).

References

Baker, J.W. (2007), "Quantitative classification of near-fault ground motions using wavelet analysis", *Bull. Seismol. Soc. America*, **97**(5), 1486-1501. http://dx.doi.org/10.1785/0120060255

Bañuelos-García, F.H., Ayala, G. and López, S. (2020), "A displacement-based seismic design procedure for buildings with fluid viscous dampers", *Earthq. Struct.*, *Int. J.*, **18**(5), 609-623. https://doi.org/10.12989/eas.2020.18.5.609

Barnes, H.A. (1989), "Shear-thickening ("Dilatancy") in suspensions of nonaggregating solid particles dispersed in Newtonian liquids", *J. Rheol.*, **33**(2), 329-366. https://doi.org/10.1122/1.550017

Bidgoli, M.R., Kolahchi, R. and Karimi, M.S. (2016), "An experimental study and new correlations of viscosity of ethylene glycol-water based nanofluid at various temperatures and different solid concentrations", *Struct. Eng. Mech.*, *Int. J.*, **58**(1), 93-102. https://doi.org/10.12989/sem.2016.58.1.093

Chen, P.C., Ting, G.C. and Li, C.H. (2020), "A versatile small-scale structural laboratory for novel experimental earthquake engineering", *Earthq. Struct.*, *Int. J.*, **18**(3), 337-348. http://dx.doi.org/10.12989/eas.2020.18.3.337

Cheng, M.Y. and Prayogo, D. (2014), "Symbiotic organisms search: A new metaheuristic optimization algorithm", *Comput. Struct.*, **139**, 98-112. https://doi.org/10.1016/j.compstruc.2014.03.007

Constantinou, M.C. and Symans, M.D. (1993), "Experimental study of seismic response of buildings with supplemental fluid dampers", *Struct. Des. Tall Build.*, **2**(2), 93-132. https://doi.org/10.1002/tal.4320020203

Crivellaro, C. and Donha, D.C. (2008), "Discrete-time dynamic model of a magneto-rheological damper for semi-active control design", *ABCM Symposium Series in Mechatronics*, Vol. 3, pp. 27-36.

Ghaffarzadeh, H. (2013), "Semi-active structural fuzzy control with MR dampers subjected to near-fault ground motions having forward directivity and fling step", *Smart Struct. Syst.*, *Int. J.*, **12**(6), 595-617. http://dx.doi.org/10.12989/sss.2013.12.6.595

Guler, E. and Alhan, C. (2019), "Effectiveness of non-linear fluid viscous dampers in seismically isolated buildings", *Earthq. Struct.*, *Int. J.*, **17**(2), 191-204. https://doi.org/10.12989/eas.2019.17.2.191

Hoffman, R.L. (1974), "Discontinuous and dilatant viscosity behavior in concentrated suspensions. II. theory and experimental tests", *J. Colloid Interf. Sci.*, **46**(3), 491-506. https://doi.org/10.1016/0021-9797(74)90059-9

Huang, X. (2018), "Evaluation of genetic algorithms for the optimum distribution of viscous dampers in steel frames under strong earthquakes", *Earthq. Struct.*, *Int. J.*, **14**(3), 215-227. https://doi.org/10.12989/eas.2018.14.3.215

Khater, H.M. (2016), "Nano-Silica effect on the physico-mechanical properties of geopolymer composites", *Adv. Nano Res.*, *Int. J.*, **4**(3), 181-195. https://doi.org/10.12989/anr.2016.4.3.181

Kurino, H., Tagami, J., Shimizu, K. and Kobori, T. (2003), "Switching oil damper with built-in controller for structural control", *J. Struct. Eng.*, **129**(7), 895-904. https://doi.org/10.1061/(ASCE)0733-9445(2003)129:7(895)

Lewandowski, R., Slowik, M. and Przychodzki, M. (2017), "Parameters identification of fractional models of viscoelastic dampers and fluids", *Struct. Eng. Mech.*, *Int. J.*, **63**(2), 181-193. https://doi.org/10.12989/sem.2017.63.2.181

Linderman, L.E. and Spencer Jr., B.F. (2015), "Closed-loop structural control with real-time smart sensors", *Smart Struct. Syst.*, *Int. J.*, **16**(6), 1147-1167. http://dx.doi.org/10.12989/sss.2015.16.6.1147

Oncu-Davas, S. and Alhan, C. (2019), "Probabilistic behavior of semi-active isolated buildings under pulse-like earthquakes", *Smart Struct. Syst.*, *Int. J.*, **23**(3), 227-242. https://doi.org/10.12989/sss.2019.23.3.227

Providakis, C.P. (2008), "Effect of LRB isolators and supplemental viscous dampers on seismic isolated buildings under near-fault excitations", *Eng. Struct.*, **30**(5), 1187-1198. https://doi.org/10.1016/j.engstruct.2007.07.020

Spencer Jr., B.F., Dyke, S.J., Sain, M.K. and Carlson, J.D. (1997), "Phenomenological model of a magnetorheological damper", *J. Eng. Mech.*, **123**(3), 230-238. https://doi.org/10.1061/(ASCE)0733-9399(1997)123:3(230)

Wei, M., Lin, K., Guo, Q. and Sun, H. (2019), "Characterization and performance analysis of a shear thickening fluid damper", *Measure. Control*, **52**(1-2), 72-80. https://doi.org/10.1177/0020294018819543

Yeh, F.Y., Chang, K.C., Chen, T.W. and Yu, C.H. (2014), "The dynamic performance of a shear thickening fluid viscous damper", *J. Chinese Inst. Engineers*, **37**(8), 983-994. https://doi.org/10.1080/02533839.2014.912775

Zapateiro, M., Luo, N., Taylor, E. and Dyke, S.J. (2010), "Modeling and identification of a class of MR fluid foam dampers", *Smart Struct. Syst.*, *Int. J.*, **6**(2), 101-113. http://dx.doi.org/10.12989/sss.2010.6.2.101

Zhao, Q., He, Y., Yao, H. and Wen, B. (2018), "Dynamic performance and mechanical model analysis of a shear thickening fluid damper", *Smart Mater. Struct.*, **27**(7), 075021. https://doi.org/10.1088/1361-665X/aac23f